GRAPHENE NANORIBBON ARRAY FABRICATION BY OXYGEN GAS PLASMA ETCHING THROUGH SUB-MICROMETER POROUS FILTERS

An Undergraduate Thesis Presented

to the Academic Faculty

by

David Shaw

In Partial Fulfillment of Institute Requirements for the Degree

B.S. in Applied Physics with Research Option

August 2009

Georgia Institute of Technology

School of Physics

GRAPHENE NANORIBBON ARRAY FABRICATION BY OXYGEN GAS PLASMA ETCHING THROUGH SUB-MICROMETER POROUS FILTERS

Approved by:

Dr. W.A. de Heer, Advisor date

Dr. Claire Berger, Advisor date

Dr. Edward Conrad, Undergraduate Coordinator date

Abstract

We investigate a novel method of fabricating a network of graphene nanoribbon structures. The process is a sharp departure from conventional nanolithographic techniques in both method and amount of time required. Epitaxial graphene prepared on single crystal 4H-SiC($000\bar{1}$) was etched with O_2 plasma through 0.2 μm porous filters adhered to the surface of the sample. Thickness measurements using ellipsometry and topological mappings using atomic force microscopy were conducted to ascertain the extent of graphene nanoribbon formation. Sheet resistance of the samples was measured using the four-point van der Pauw method to ensure the existence of electrical conductivity in the etched samples. Furthermore, the etch-rate of multilayer epitaxial graphene was determined.

Contents

1 Introduction

1.1 Literature Review

The phenomenal electronic transport properties of graphene - a two-dimensional honeycomb lattice of carbon atoms - have recently captured the interests of all major research institutions and leaders of the semiconducting industry. Graphene appears to have retained many of the electronic capabilities observed in carbon nanotubes (CNTs) - cylindrical structures of a single graphene sheet - without their drawbacks. CNTs have been shown to exhibit metallic or semiconducting properties depending on their geometry [1]. However, producing CNTs in a controlled manner has yet to be established; current methods amount to sifting through the carbon soot of an arc discharge [2]. Furthermore, the electronic properties cannot be ascertained unless scanning tunneling microscopy (STM) is used to map the helicity of a CNT, which is often destructive to the surface of the sample. Assembling a device with components of unknown properties is an unrealistic goal. It is not surprising that graphene has succeeded CNTs as the dominating graphitic structure in recent publications; however, it is not just its rolled-up counterpart that graphene seeks to overthrow.

In the microelectronics industry, silicon is the backbone of transistor-device fabrication. Its chemical properties make silicon the ideal material to use in doping applications to control the number and charge of current carriers [3]. As time progresses, transistor devices shrink. Moore's law states that the number of transistors that can be placed inexpensively on an integrated circuit (IC) increases exponentially with time [4]. This trend, which corresponds to a doubling every two years, was first elucidated by Intel cofounder Gordon E. Moore in 1965. Intel has buttressed the exponential growth with its new Quad-Core Itanium Tukwila processor, an astonishing device that packs two billion transistors to a single IC [5]. Intel has utilized 65 nm process technology to lithographically pattern silicon wafers to these minute scales. This corresponds to transistor separation on the order of the width of approximately 300 atoms. It quickly becomes obvious that Moore's law cannot be sustained indefinitely; a fundamental limit must exist. A silicon transistor cannot be minimized beyond the realm of nano-scale dimensions; after all, a transistor is fundamentally composed of silicon atoms. Experts predict this scale will be reached in perhaps 10-15 years. New technologies are being investigated to stave off this inevitable slackening in Moore's law. Molecular assembly of transistors holds promise, yet it is decades away. Graphene is a possible successor because it can do everything that silicon can, but better. It is the hope of graphene researchers, especially those of the Materials Research Science and Engineering Center (MRSEC) here at Georgia Tech, for graphene, with its superior electronic properties, to advance the emerging limitations of silicon-based transistor devices and to sustain Moore's law.

The current fabrication processes of graphene make it suitable for large-scale integration into transistor devices. The epitaxial method of thermal decomposition of SiC is capable of producing multiple samples at a time. These macroscopic planar samples are extended two-dimensionally, not just along one (nano-scale) dimension as with CNTs [6].

The charge carriers in graphene have been shown to exhibit ballistic scattering - an unimpeded flow of charge over relatively long distances [7]. The charge carriers, whether electrons or holes, behave like massless Dirac fermions and travel through the system with a velocity on the order of 10^6 m/s, which is the Fermi velocity v_F [7]. This behavior is observed at room temperature. In addition, some of the highest carrier mobilities μ in any material have been observed in graphene. The mobility of silicon has been measured at 1,500 $\frac{cm^2}{Vs}$; this value is at least an order of magnitude greater at 15,000 - 100,000 $\frac{cm^2}{Vs}$ in graphene [6].

These numbers alone demonstrate the vast potential for graphene-based transistor devices. However, to be competitive in this field, semiconducting graphene must be demonstrated. Its energy band structure classifies graphene as a zero-gap semiconductor [7]. The energy diagram of the conduction and valence bands depicts a linear-dispersion relation in which the bands meet at a centralized focus referred to as the Dirac point [8]. The characteristic energy gap between the conduction and valence bands observed in standard semiconductors does not exist in graphene. Recent research has demonstrated that sizeable energy gaps can be tuned in graphene by physically reducing the size of a sample [8]. Minimizing the width of a graphene sample to nano-scale

proportions results in observable energy gaps similar to those intrinsically found in silicon and gallium arsenide [3]. To be effective, a graphene nanoribbon (GNR) must be lithographically patterned to widths smaller than 5nm, substantiating the one-over-the-width band gap dependence [8].

Recently, novel methods of creating GNRs have emerged. Li et al pioneered a solution-phase derived method which produced sub-10 nm GNRs [9]. Oxygen gas plasma etching has been utilized to a certain extent; however, fabricating GNRs smaller than 20 nm with this method has not been accomplished [10]. The standard lithographic patterning method using scanning electron microscopy (SEM) has been widely used, especially by de Heer *et al*, to create GNRs with widths of a few tens of nanometers [11]. However, this process requires hours to complete; therefore, a method is needed to obtain the results of lithographic patterning with potential for large-scale integration in transistor devices.

The semiconductor industry has demonstrated the need for a new technology to sustain the performance of transistor devices. Well documented evidence shows that large-scale production of GNRs can catapult this performance to unprecedented levels.

1.2 Theory

1.2.1 Semiconductor Energy Band Structure

The electronic properties of most solids can be categorized as being either insulating or metallic. The electron states of allowable energies dictate a material's energy band structure. An insulator's energy band structure is characterized by a region of forbidden energies between the top of the highest filled (valence) bands and the bottom of the lowest empty (conduction) bands, where the forbidden region corresponds to the energy gap E_g. The boundary between the valence and conduction bands of a metallic solid occurs within a region of allowed energies; thus, the characteristic energy gap is not observed in metals.

The magnitude of the energy gap governs the probability of conduction in an insulator. As temperature is increased, electrons are thermally excited across the band gap into the unoccupied conduction bands in which conduction is carried out by these thermally excited electrons as well as by the "holes"

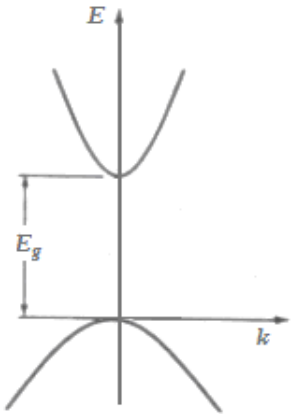

Figure 1. Energy band structure of an arbitrary insulator.

the electrons left behind in the valence band. The fraction of electrons excited across the energy gap is given by the approximate Boltzmann distribution

$$\exp(-E_g/2k_BT), \tag{1}$$

where k_B is the Boltzmann constant [12]. From this distribution it can be seen that observable conduction at room temperature occurs only if the band gap is on the order of a few electron volts. The aforementioned sentence serves to define the murky distinction between insulators and semiconductors, which, as defined by Ashcroft and Mermin, are, "Solids that are insulators at T = 0, but whose energy gaps are of such a size that thermal excitation can lead to observable conductivity at temperatures below the melting point [12]." An energy-momentum plot is depicted in Figure 1 demonstrating a single valence and conduction band of an arbitrary insulator.

If the band gap of Figure 1 was of sufficient magnitude, perhaps 1.1 eV, then this energy band structure would represent silicon.

Semiconductors are the predominant material used in the microelectronics industry due to their unique, inherent properties; notably, the phenomenon that a semiconductor's conductivity increases with increasing temperature. Furthermore, the ability to control the flow of charge carriers through doping the material or an applied electric field adapts a semiconductor to myriad uses. The following section elucidates the energy band structure of graphene and its application to semiconductors.

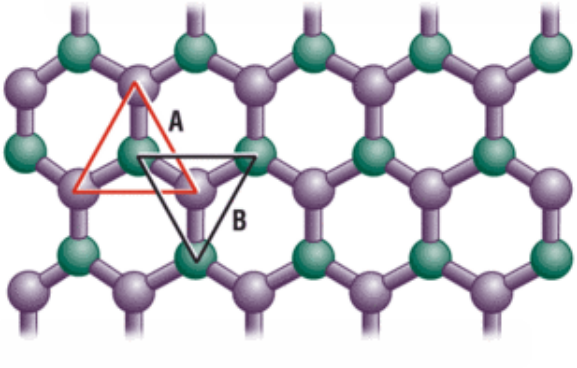

Figure 2. Orientation of triangular sublattices A and B relative to carbon honeycomb lattice.

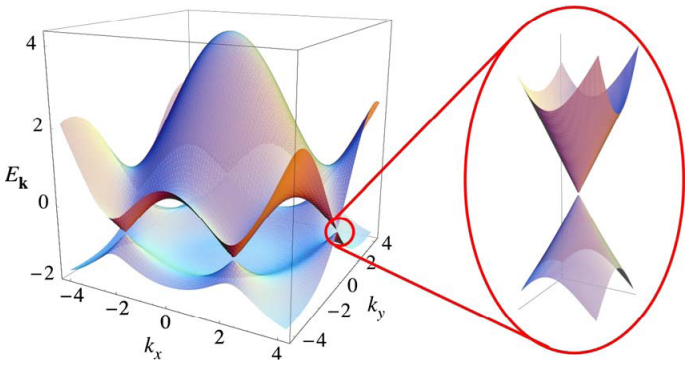

Figure 3. Graphene energy band structure over the entire Brillouin Zone.

1.2.2 The Energy Band Structure of Graphene

The characteristic linear dispersion relation displayed by graphene stems from the inherent symmetry of the crystal lattice of carbon atoms [7]. The sp^2 hybridized carbon bonds, consisting of three sigma (σ) bonds and one pi (π) bond per carbon atom, account for graphene's renowned in-plane strength as well as its conducting properties [13]. The π orbitals, each orthogonal to the plane of σ bonds, provide the electrons that are responsible for conduction within the system. The honeycomb lattice is further decomposed into two triangular sublattices A and B, as illustrated in Figure 2. The associated reciprocal lattice vectors define the graphene Brillouin Zone, a region in which the electronic behavior represents that of the entire honeycomb lattice. The two-dimensional energy dispersion relation is obtained from the tight-bonding Dirac-like hamiltonian

$$\widehat{H} = \hbar v_F \begin{pmatrix} 0 & f(\boldsymbol{k}) \\ -f^{\dagger}(\boldsymbol{k}) & 0 \end{pmatrix}, \qquad (2)$$

where v_F is the Fermi velocity and $\boldsymbol{k}$ is the momentum wave vector of the charge carriers [7]. Solution of the eigenvalue problem yields the energy equation

$$E_{\pm} = \pm t\sqrt{3 + f(\boldsymbol{k})}, \qquad (3)$$

where

$$f(\boldsymbol{k}) = 2\cos(\sqrt{3}k_y a) + 4\cos(\frac{\sqrt{3}}{2}k_y a)\cos(\frac{3}{2}k_x a), \quad (4)$$

where $a \approx 1.42$ Å [14]. The constant term t of Eq. (3) corresponds to the nearest-neighbor hopping energy and has a value of approximately 2.7 eV. The hopping energy emanates from the overlapping π orbitals of adjacent carbon atoms. A certain probability exists that an electron will "hop" to its nearest-neighbor carbon atom; a smaller probability exists that an electron will "hop" to its next-nearest-neighbor carbon atom, and so on and so forth. These overlap energies contribute to the energy dispersion relation with each successive neighboring carbon atom contributing a smaller energy. The hamiltonian of Eq. (2), and therefore, the energy dispersion relation of Eq. (3), takes into account only the contribution of the nearest-neighbor hopping energy t. It is wise, therefore, to consider the energy dispersion relation with the added contribution of t', the next-nearest neighbor hopping energy. Eq. (3) now becomes

$$E_{\pm} = \pm t\sqrt{3 + f(\boldsymbol{k})} - t' f(\boldsymbol{k}), \qquad (5)$$

where t' is approximately 0.1 eV, a small but noticeable contribution [14]. The plus and minus signs correspond to the π^* (conduction) and the π (valence) energy bands, respectively.

Figure 3 depicts the energy dispersion relation through the whole region of the graphene Brillouin Zone. This band structure is obtained by expanding Eq. (5) about one of two special points of interest, the K- or K'- point. The blown-up portion of Figure 3 focuses on one of these points, referred to as Dirac points, located at the six corners of the Brillouin Zone. These Dirac points, connecting the π^* and π bands in a linear dispersion relation at a Fermi

surface at $E = 0$, give rise to the unique physics observed in graphene.

The linear nature of the energy bands near the Dirac points, described by the energy equation

$$E = \hbar \boldsymbol{k} v_F, \tag{6}$$

enables the electrons to behave like massless Dirac fermions. Furthermore, the chirality of the system prohibits charge carriers belonging to the same curve of the linear energy dispersion from hopping to the intersecting linear energy curve within the same Dirac cone. This is due to the fact that the pseudospin σ of the charge carriers is not conserved and establishes the basis for the phenomenon of ballistic scattering observed in graphene [13].

1.2.3 Graphene's Inverse-Width Energy Gap Dependence

As Kim *et al* have demonstrated that sizeable Energy gaps scale inversely with GNR width, it is useful to establish a theoretical foundation for this claim, albeit an approximate one.

Beginning with Eq. (6), the wave vector $\boldsymbol{k}$ can be decomposed into its two-dimensional components k_x and k_y as

$$\boldsymbol{k} = \sqrt{k_x^2 + k_y^2}. \tag{7}$$

Next, the standing waves of a particle confined within a potential square-well are given by

$$\lambda = \frac{2W}{n}, \tag{8}$$

where λ is the wavelength, W is the width of the potential well and n is the energy level. The wavenumber k can be expressed as

$$k = \frac{2\pi}{\lambda}. \tag{9}$$

Combining Eqs. (8) and (9) yields

$$k = \frac{n\pi}{W}. \tag{10}$$

If we model a GNR after a particle confined within a potential well, and designate the y-axis as the transmission axis of charge carriers, we can neglect the k_x component of $\boldsymbol{k}$. Eq. (10) can be substituted for $\boldsymbol{k}$ of Eq. (6), giving

$$E = \hbar v_F \left(\frac{n\pi}{W} \right). \tag{11}$$

It is evident from Eq. (11) that altering a GNR's width will produce a change in energy that is manifested as an energy gap between the π^* and π bands. Recent studies have revealed that 15 nm wide lithographically patterned GNRs can achieve energy gaps of $\approx 0.2\ eV$ [8].

1.3 The Conventional Nanolithography Process

While variations exist in patterning semiconducting materials, electron-beam (e-beam) lithography appears to be the method of choice when patterning graphene samples to nano-scale proportions [15-17]. In this process, either a positive or negative photoresist is applied evenly to the surface of the substrate; the positive and negative designation merely determines whether the developed regions perish or persist, respectively, upon exposure. The material poly(methyl methacrylate) (PMMA), a synthetic polymer of methyl methacrylate, dissolved in a liquid solvent is the standard positive e-beam resist used for patterning applications. Irrespective of type, a photoresist is spin coated onto the substrate to ensure an even distribution where film thicknesses achieve depths of several hundreds of nm. Heat is then applied to the substrate to bake out the casting solvent. A scanning electron microscope (SEM) is used to expose the photoresist in a predetermined pattern; in the case of PMMA, exposure entails breaking the polymer into fragments. The final step requires the sample to be immersed in a developer, usually a solution composed of methyl isobutyl ketone (MIBK) and isopropyl alcohol (IPA) in a one-to-three ratio, that dissolves the exposed regions.

Depending on the application, further steps may be required to complete the process, such as plasma etching and wire-bonding. These additional steps only add to the hours required to lithographically pattern a substrate. For graphene to prove a viable semiconducting material, large-scale production must be demonstrated. The following sections detail a promising step in that direction.

2 Methods

2.1 Experiment Feasibility

PMMA coated Si(100) substrates were initially experimented on to determine the difference in etch-rate of PMMA between samples directly exposed to an O_2 plasma and samples shielded from direct exposure with a porous filter. This step was taken to ascertain the viability of the experiment without consuming valuable graphene samples: if the porous filters prohibited the oxygen ions from reacting with the PMMA surface, there would be no point in continuing the experiment.

All Si substrates (samples P4, P5, P6, P7, P10 and P11) were spin coated with PMMA for 60 seconds at 5,000 rpm followed by a 90 second bake at 180°C to set the thermoplstic. This duration and rate produced an average PMMA film thickness of $\approx$ 650 nm. Thickness measurements were performed with a HORIBA Jobin Yvon AUTO SE ellipsometer.

Following the spin coating, samples P4, P5 and P6 were etched in a SAMCO model RIE-1C reactive ion etching (RIE) system with an O_2 flow rate of 4 standard cubic centimeters per minute (sccm) at a radio frequency (RF) power of 16 W for a duration of one minute. Table 1 in the Results and Analysis section displays the thicknesses of these samples obtained from the ellipsometer.

Additionally, samples P7, P10 and P11 were adhered to 25 mm wide, 60 μm thick Whatman Anopore aluminum oxide (Anodisc) membranes with a pore size of 0.2 μm, as shown in Figure 4. The filter-sample assemblies were then etched with the RIE at the aforementioned parameters. The filters were then removed for PMMA thickness measurements. Table 2 in the Results and Analysis section contains the data of initial and final thicknesses. [1]

As an aside, while the purpose of this experiment is not to *uniformly* etch the PMMA below the filter, but rather, to see if *any* etching occurs, the differential PMMA etch-rate that arises from etching through a filter as opposed to no filter can give some insight into whether the experiment is on the right path: the ellipsometer measures the average thickness of a 250 μm x 250 μm region of the sample; therefore, if oxygen ions are able to react with the PMMA through the pores of the filter, then one would expect the ellipsometer to register a change in the average thickness of PMMA, albeit a small one. If only certain areas of the PMMA were etched, such as immediatley below the pores (in the event of GNR formation), the thickness of the PMMA would still decrease as measured by the ellipsometer as it takes an average measurement.

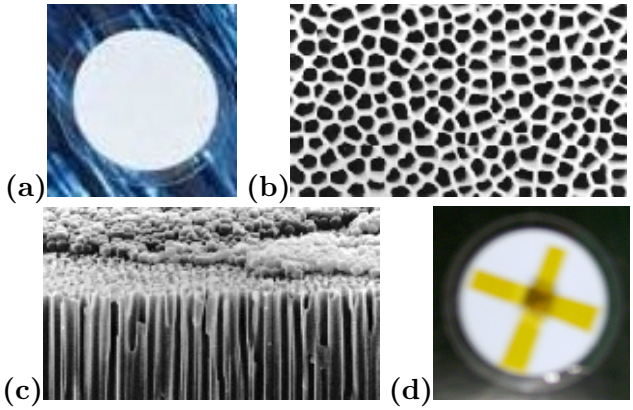

Figure 4. (a) Macroscopic image of a Whatman Anodisc filter. (b) Magnified top-view of 0.2 μm Anodisc filter demonstrating pore distribution. (c) Cross-sectional view of 0.2 μm Anodisc filter showing pore structure. (d) Filter-sample assembly.

2.2 Graphene Etching

The results of the previous section were used to determine the necessary length of time for oxygen ions to react with the graphene layers during etching through an Anodisc filter. Epitaxial graphene sample C1515 was prepared on H_2 etched 4H-SiC($000\bar{1}$) (carbon-face) and measured using ellipsometry. This sample was then directly subjected to an O_2 plasma in the RIE with an O_2 flow rate of 4 sccm at a power of 16 W for a duration of 5 seconds. Table 3 in the Results and Analysis section provides the initial and final thickness as well as the previously unknown etch-rate of graphene.

It was determined from the ratio of the difference in PMMA etch-rates that a 0.2 μm filter impedes the etching of PMMA by a factor of 14. This logic was applied to the etch-rate of graphene to justify a duration of plasma etching through a 0.2 μm filter attached to a graphene sample. Sample C1532, a graphene sample prepared on H_2 etched 4H-SiC($000\bar{1}$), was adhered to the Anodisc filter and

[1] All PMMA thickness measurements were averaged over four locations throughout a given sample.

Table 1. Thickness measurements of PMMA on Si substrates before (T_i) oxygen plasma etching and after (T_f).

Sample	T_i (nm)	T_f (nm)	Etch-rate (nm/m)
P4	621.15	359.25	261.90
P5	645.05	379.70	265.35
P6	613.45	355.25	258.20

Table 2. Thickness measurements of PMMA on Si substrates before (T_i) oxygen plasma etching through 0.2 μm Anodisc filter and after (T_f).

Sample	T_i (nm)	T_f (nm)	Etch-rate (nm/m)
P7	668.48	649.96	18.52
P10	637.93	624.29	13.64
P11	646.18	637.69	8.49

Table 3. Thickness measurements of graphene on SiC substrate before (T_i) oxygen plasma etching and after (T_f).

Sample	T_i (Å)	T_f (Å)	Etch-rate (Å/s)
C1515	14.84	5.95	8.89

etched with an O_2 flow rate of 4 sccm at a power of 16 W for 480 seconds.

Finally, sample C1733, a graphene sample grown on 4H-SiC(000$\bar{1}$), was etched in a similar fashion (adhered to 0.2 μm Anodisc filter) as sample C1532, but at a power of 36 W for a duration of 720 seconds.

3 Results and Analysis

3.1 Experiment Feasibility

As Tables 1 and 2 demonstrate, the difference in etch-rate between PMMA coated Si samples etched by direct exposure to an oxygen plasma (average etch-rate $\approx$ 262 nm/m), or through an Anodisc filter (average etch-rate $\approx$ 14 nm/m), is clearly observed.

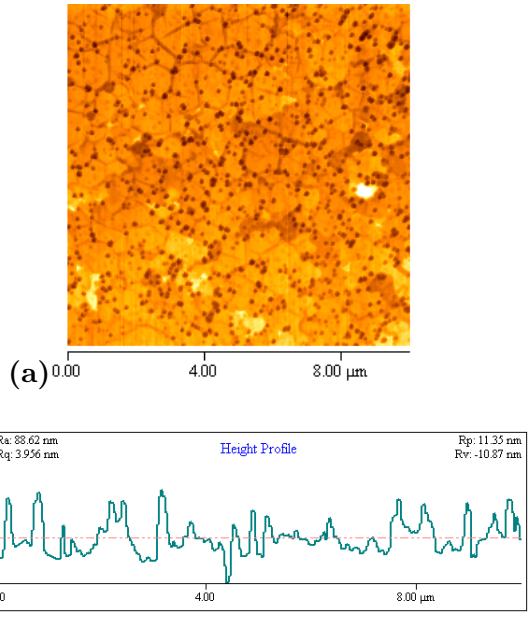

Figure 5. (a) AFM image of sample C1532. (b) Height profile analysis of sample C1532.

It is evident from Table 2 that etching through a 0.2 μm filter greatly reduces the etch-rate; however, this has proved that the oxygen ions did indeed react with the PMMA, and, by association, would react with graphene, as well.

3.2 Graphene Etching

3.2.1 Sample C1515

Experimentation on sample C1515 stemmed from the wish to determine the oxygen plasma etch-rate of graphene. Table 3 depicts the final result as being 8.89 Å/second at the etching-parameters mentioned in the Methods section. This etch-rate represents an average value as a 15 point ellipsometric thickness measurement was conducted. The initial thickness and final thickness listed in Table 3 represent the average of the 15 measurements taken.

3.2.2 Sample C1532

Sample C1532 yielded the most promising results for exhibiting GNR-like structures. Figure 5 shows an atomic force microscopy (AFM) topological mapping of the surface of C1532 following its plasma etch through the Anodisc filter. Of interest are the random fluctuations in elevation that appear randomly throughout the sample. The height profile analysis shows an array of disordered peaks and valleys

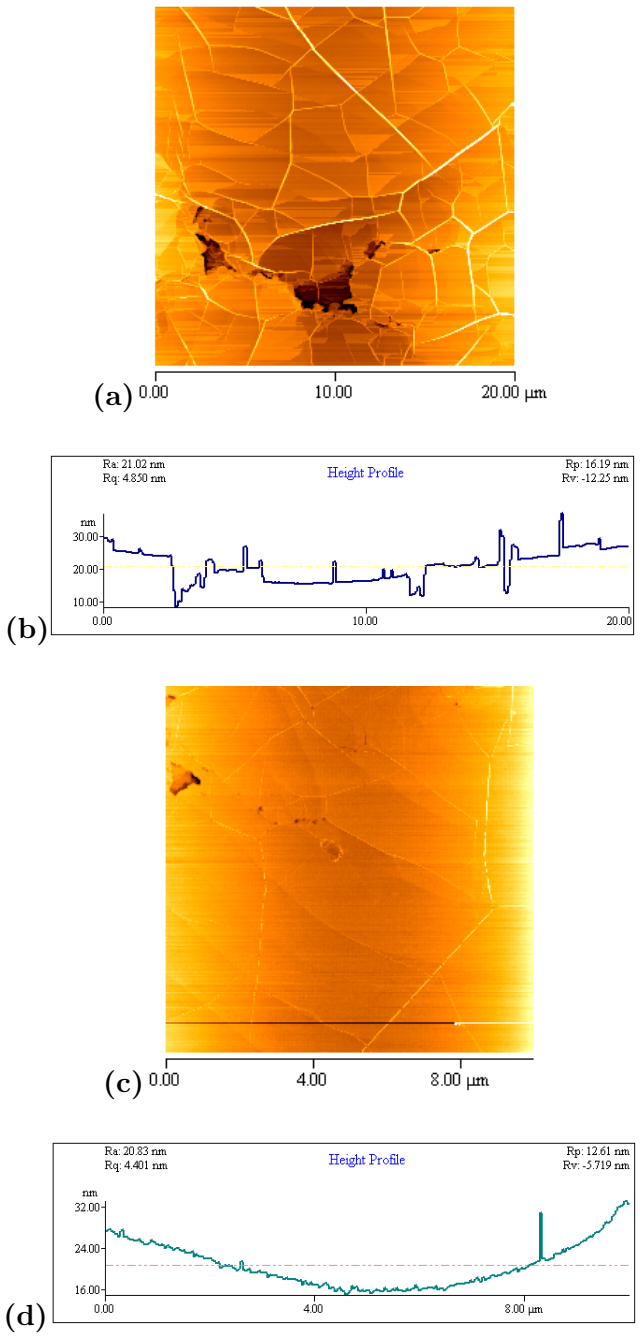

Figure 6. (a) AFM image of sample C1733 before oxygen plasma etch. (b) Height profile analysis of sample C1733 before plasma etch. (c) AFM image of sample C1733 after plasma etch. (d) Height profile analysis of sample C1733 after plasma etch.

that appear to be a few hundred nm wide. However, while the four-point van der Pauw method was applied to determine that the sample was still conducting, it is not clear as to whether the graphene has etched completely through to the SiC substrate in the valleys.

3.2.3 Sample C1733

Graphene sample C1733 showed little evidence of GNR formation. Figure 6 demonstrates AFM images of the surface both prior to and after etching through the Anodisc filter. The associated height profiles are included in Figure 6, as well. A plausible explanation for the absence of any structural ribbons may be that the power (36 W) and duration (720 seconds) of the plasma etching were too high. This could have manifested as an over-abundance of oxygen ions penetrating through the filter, causing uniform etching of graphene. This claim may be supported in the AFM images of Figure 6. Extensive pleating of the pre-etched graphene surface of Figure 6 (a) is visible. This extensive pleating is not visible in Figure 6 (c), which is the post-plasma-etched AFM image. The higher-energy ions (as compared to those created by a RF power of 16 W) may have uniformly etched away at the graphene layers, leaving behind a less-pleated surface. This claim is further buttressed as ellipsometric analysis reveals that approximately half of the graphene layers were etched, as shown in Table 4. In addition, the four-point van der Pauw method confirmed that the sample was still conducting with a restivity of 240 ohms/square.

Table 4. Thickness measurements of graphene sample C1733 before (T_i) oxygen plasma etching and after (T_f).

Sample	T_i (Å)	T_f (Å)
C1733	34.15	15.65

4 Conclusion

The scope of this paper has aimed to delineate a novel approach to fabricating GNRs. It was demonstrated that conventional nanolithography techniques, while effective, are not suited for large-scale production of graphene-based electronics. The method outlined in this paper can, in terms of time, be counted in seconds as opposed to hours. Furthermore, this method allows for the simultaneous patterning of multiple samples.

While the facts in this paper supporting the fabrication of GNRs using this method are not ironclad, a framework upon which future research can build upon has been created.

Acknowledgements

I wish to thank Dr. W.A. de Heer and Dr. Claire Berger for allowing me to participate in the Epitaxial Graphene Laboratory and the groundbreaking research that occurs there. Their guidance and willingness to assist, as well as the advice from lab members Dr. Xiasong Wu, John Hankison, Mike Sprinkle, Ming Ruan, Yike Hu and Karine Madiomanana, have been instrumental in the completion of this paper.

References

[1] P. McEuen, "Single-wall carbon nanotubes," *Physics World*, vol. 13, no. 6, pp. 31-36, Jun. 2000.

[2] S. Iijima, "Carbon Nanotubes," *Solid State Physics*, vol. 27, no. 6, pp. 39-45, 1992.

[3] W. C. O'mara, *Handbook of Semiconductor Silicon Technology.* New York: Noyes, 1990.

[4] G. E. Moore, "Cramming more components onto integrated circuits," *Electronics*, vol. 38, no. 8, Apr. 1965.

[5] C. Kowaliski, "Quad-core Itanium packs 2 biliion transistors," *The Tech Report*, http://techreport.com/discussions.x/14066.

[6] J. Kedzierski, "Epitaxial Graphene Transistors on SiC Substrates," *IEEE Transactions on Electronic Devices*, vol. 55, no. 8, Aug. 2008.

[7] A.K. Geim and K.S. Novoselov, "The rise of graphene," *Nature Materials*, vol. 6, pp. 183-191, Mar. 2007.

[8] P. Kim, "Energy Band-Gap Engineering of Graphene Nanoribbons," *Physical Review Letters*, vol. 98, pp. 206805-1 - 4, May 2007.

[9] X. Li, "Chemically Derived, Ultrasmooth Graphene Nanoribbon Semiconductors," *Science Express*, vol. 10, Jan. 2006.

[10] Xinran Wang, Yijian Ouyang, Xiaolin Li, Hailiang Wang, Jing Guo and Hongjie Dai1, "Room-Temperature All-Semiconducting Sub-10-nm Graphene Nanoribbon Field-Effect Transistors," *Physical Review Letters*, vol. 100, May 2008.

[11] W. A. de Heer, C. Berger, X. Wu, P. N. First, E. H. Conrad, X. Li, T. Li, M. Sprinkle, J. Hass, M. L. Sadowski, M. Potemski, and G. Martinez, "Epitaxial graphene," *Solid State Commun.*, vol. 143, no. 1/2, pp. 92-100, Jul. 2007.

[12] N. W. Ashcroft and N. D. Mermin, *Solid State Physics.* Philadelphia: Saunders College, 1976.

[13] J. Hass, W. A. de Heer and E.H. Conrad, "The growth and morphology of epitaxial multilayer graphene," *J. Phys.:Condens. Matter*, vol. 20, Jul. 2008.

[14] A. H. Castro Neto, F. Guinea, N. M. R. Peres, K. S. Novoselov and A. K. Geim, "The electronic properties of graphene," *Reviews of Modern Physics*, vol. 81, Jan. 2009.

[15] N. Camara, G. Rius, J.R. Huntzinger, A. Tiberj, N. Mestres, P. Godignon and J. Carnassel, "Selective epitaxial growth of graphene on SiC," *Applied Physics Letters*, vol. 93, Sep. 2008.

[16] T. Moriki, A. Kanda, T. Sato, H. Miyazaki, S. Odaka, Y. Ootuka, Y. Aoyagi and K. Tsukagoshi, "Electron transport in thin graphite films: Influence of microfabrication processes," *Science Direct*, vol. E 40, pp. 241-244, Jun. 2007.

[17] M. Han, B. Ozyilmaz, Y. Zhang, P. Jarillo-Herero and P. Kim, "Electronic transport measurements in graphene nanoribbons," *phys. stat. sol.*, vol. 244, no. 11, pp. 4134-4137, Oct. 2007.